

THE HUBBLE DIAGRAM OF
THE CALÁN/TOLOLO TYPE Ia SUPERNOVAE
AND THE VALUE OF H_0

Mario Hamuy^{1,2}
M. M. Phillips¹
Nicholas B. Suntzeff¹
Robert A. Schommer¹
José Maza³
R. Avilés¹

¹ National Optical Astronomy Observatories*, Cerro Tololo Inter-American Observatory, Casilla 603, La Serena, Chile

² University of Arizona, Steward Observatory, Tucson, Arizona 85721

³ Departamento de Astronomía, Universidad de Chile, Casilla 36-D, Santiago, Chile

electronic mail: mhamuy@as.arizona.edu, mphilips@noao.edu,
nsuntzeff@noao.edu, rschommer@noao.edu, jmaza@das.uchile.cl

Running Page Head : HUBBLE DIAGRAM OF SNe Ia

Address for proofs: M. M. Phillips, CTIO, Casilla 603, La Serena, Chile

Key words: photometry - supernovae -

*Cerro Tololo Inter-American Observatory, National Optical Astronomy Observatories, operated by the Association of Universities for Research in Astronomy, Inc., (AURA), under cooperative agreement with the National Science Foundation.

ABSTRACT

The Calán/Tololo supernova survey has discovered ~ 30 Type Ia supernovae at redshifts out to $z \sim 0.1$. Using $BV(I)_{KC}$ data for these objects and nearby SNe Ia, we have shown that there exists a significant dispersion in the intrinsic luminosities of these objects. We have devised a robust χ^2 minimization technique simultaneously fitting the BVI light curves to parametrize the SN event as a function of $(t_B, m_i, \Delta m_{15}(B))$ where t_B is the time of B maximum, m_i is the peak BVI magnitude corrected for luminosity variations, and $\Delta m_{15}(B)$ is a single parameter describing the *whole* light curve morphology. When properly corrected for $\Delta m_{15}(B)$, SNe Ia prove to be high precision distance indicators, yielding relative distances with errors $\sim 7\text{-}10\%$. The corrected peak magnitudes are used to construct BVI Hubble diagrams, and with Cepheid distances recently measured with the Hubble Space Telescope to four nearby SNe Ia (1937C, 1972E, 1981B, and 1990N) we derive a value of the Hubble constant of $H_0 = 63.1 \pm 3.4$ (internal) ± 2.9 (external) $\text{km s}^{-1} \text{Mpc}^{-1}$. This value is $\sim 10\text{-}15\%$ larger than the value obtained by assuming that SNe Ia are perfect standard candles. As we have shown in Paper V, there is now strong evidence that galaxies with younger stellar population (spirals and irregulars) appear to host the slowest-declining, and therefore most luminous SNe Ia. Hence, the use of Pop I objects such as Cepheids to calibrate the zero point of the SNe Ia Hubble diagram can easily bias the results toward luminous SNe Ia, *unless the absolute magnitude-decline relation is taken into account*.

Using the inertial reference frame of the distant SNe Ia, and the "corrected" apparent magnitudes of the best observed SNe Ia in the Virgo and Fornax clusters, we have evaluated the recession velocities of these two clusters based on the Calán/Tololo Hubble diagrams. We find a cosmic recession velocity for Virgo of $1,223 \pm 115 \text{ km s}^{-1}$ and for Fornax of $1,342 \pm 70 \text{ km s}^{-1}$, and a relative distance modulus of $\Delta\mu(\text{Fornax-Virgo}) = 0.19^m \pm 0.23^m$.

1 Introduction

In mid-1990, a group of astronomers of the Cerro Tololo Inter-American Observatory (CTIO) and the University of Chile at Cerro Calán initiated a photographic search for supernovae with the aim of producing a moderately distant ($0.01 \lesssim z \lesssim 0.1$) sample suitable for cosmological studies. The technique employed in our survey was described in detail by Hamuy *et al.* 1993a (Paper I). In the course of 1990-93 this project led to the discovery of 50 SNe ($\sim 1/3$ of all of the SNe discovered throughout the world in the same period). Followup spectroscopic observations revealed that 32 of these objects were members of the Type Ia class, the majority of which were found near maximum light.

Thanks to the generous collaboration of many visiting astronomers and CTIO staff members, we were able to gather $BV(RI)_{KC}$ CCD photometry for 27 of these Calán/Tololo SNe Ia. Preliminary light curves and spectroscopy were published in Paper I, Paper II (Maza *et al.* 1994), and Paper III (Hamuy *et al.* 1994) for six events. Based on photometry for 13 of the Calán/Tololo SNe Ia, in Paper IV (Hamuy *et al.* 1995) we discussed the Hubble diagrams in B and V. The latter study confirmed, in general terms, the finding by Phillips (1993) that the absolute B and V magnitudes of SNe Ia are correlated with the initial decline rate of the B light curve. In addition, we found evidence that galaxies having a younger stellar population appear to host the most luminous SNe Ia, and pointed out that this effect could introduce significant bias into determinations of both H_o and q_o . A significant decrease in the scatter of the B and V Hubble diagrams was obtained when the data were corrected for the peak luminosity-decline rate relation, and a Hubble constant in the range $H_o = 62\text{--}67 \text{ km s}^{-1} \text{ Mpc}^{-1}$ was found using the Cepheid distance to the host galaxy of SN 1972E to derive the zero point of the Hubble relation.

We have now produced definitive light curves for the complete sample of 27 Calán/Tololo SNe Ia, and also for two additional SNe Ia found in the course of other survey programs which we included in our followup program. In an accompanying paper (Hamuy *et al.* 1996a; hereafter referred to as Paper V), we have reexamined the absolute luminosities of this full set of 29 SNe Ia. These data confirm the major conclusions of Paper IV concerning 1) the reality of the absolute magnitude-decline rate relation, and 2) the link between SNe Ia luminosities and the morphology of the host galaxies. The purpose of the current paper is to present and discuss the final versions of the Hubble diagram in B and V for the full set of Calán/Tololo SNe Ia, as well as the first Hubble diagram in the I band. After a brief description of our sample (Sec. 2), we present in Sec. 3 the resulting BVI Hubble diagrams. In Sec. 4 we discuss our results, and in Sec. 5 we summarize our conclusions.

2 The Calán/Tololo Database

Of the 32 SNe Ia discovered during the course of the Calán/Tololo survey, adequately sampled BV(I)_{KC} light curves were obtained for a total of 27 events. To this sample we have added two SNe Ia – 1990O and 1992al – which, although not found by us, were included in our program of followup photometry. Hence, the total sample of distant SNe Ia considered in this paper is 29.

In an accompanying paper (Hamuy *et al.* 1996b; hereafter referred to as Paper VII), we give the individual BV(RI)_{KC} light curves for this set of 29 SNe Ia along with details of the photometric reductions. Estimates of the maximum light magnitudes in the B, V, and I bands and the initial decline rate parameter $\Delta m_{15}(B)$ (Phillips 1993) are also provided. As discussed in Paper VII, maximum-light magnitudes were measured directly from the observations whenever possible. We were able to perform this measurement for 11 SNe for which the time of the first photometric observation was no later than day +1 (counted since the peak of the B light curve), by fitting a low-order (3-4) polynomial to the data around maximum light. For the remaining 18 objects whose followup photometric observations did not begin until after maximum light, the peak magnitudes were estimated using a robust χ^2 -minimizing fitting procedure similar to that described in Paper IV. Note, however, that in order to include the I-band data, an updated and expanded set of BV(I)_{KC} light curve templates were employed. This new set of templates are the subject of Paper VIII (Hamuy *et al.* 1996c) in this series. These templates were fit to the observed photometry of each SN solving simultaneously for the time of B maximum and the peak magnitudes B_{MAX} , V_{MAX} , and I_{MAX} . (See Paper VII for further details of this fitting procedure.)

In Table 1 we list the relevant information for this study for the 29 SNe in the following format:

Column (1): SN name

Column (2): decimal logarithm of the heliocentric radial velocity (cz) of the parent galaxy corrected to the cosmic microwave background (CMB) frame. The heliocentric redshifts were all measured from our own spectroscopic observation of the nuclei of the parent galaxies and the transformation to the CMB frame was performed by adding the vectors (-30,297,-27) and (7,-542,302) km s⁻¹ (in Galactic Cartesian Coordinates). The former is the motion of the sun with respect to the Local Group (Lynden-Bell & Lahav 1988) while the latter is the motion of the Local Group with respect to the CMB as measured with COBE (Smoot *et al.* 1992). We assigned a possible peculiar velocity component of ± 600 km s⁻¹ to each galaxy which is given in brackets in units of mdex.

Column (3), (4) and (5): the apparent B, V, and I peak magnitudes of the SN as determined from the light curves, corrected for foreground extinction in the direction of the host galaxy

(Burststein & Heiles 1982), and for the K terms calculated by Hamuy *et al.* (1993b).¹ *Note, however, that no correction has been applied for possible obscuration in the host galaxy (see Sec. 3).*

Column (6): the “color” of the SN, $B_{MAX}-V_{MAX}$.

Column (7), (8) and (9): the absolute B, V, and I peak magnitudes of the SN calculated from the apparent magnitude, the redshift of the host galaxy (in the CMB frame), and an assumed Hubble constant of $H_0 = 65 \text{ km s}^{-1} \text{ Mpc}^{-1}$. As discussed in Sec. 4 this value corresponds closely to the Hubble diagram of SNe Ia with its zero point duly calibrated with Cepheid distances to nearby SNe Ia.

Column (10): the decline rate parameter $\Delta m_{15}(B)$, defined by Phillips (1993) as the amount in magnitudes that the B light curve decays in the first 15 days after maximum light. In most cases (24 SNe) this parameter was estimated through the template fitting procedure previously described in Papers III and IV.

Column (11): an estimate (in Angstroms) of the equivalent width of Na I D interstellar absorption due to the host galaxy from the spectra of the SNe. In most cases we were only able to place an upper limit to the equivalent width based on the signal-to-noise ratio of the spectra.

3 The Hubble Diagrams in B, V, and I

Figure 1 shows the resulting Hubble Diagrams in B, V, and I for the Calán/Tololo SNe Ia data given in Table 1. The ridge lines, which correspond to (weighted) least-squares fits of the data to the theoretical lines of constant luminosity, yield the following zero points and dispersions:

$$B_{MAX} = 5 \log cz - 3.151 (\pm 0.029) \sigma = 0.38 \text{ n} = 29, \quad (1)$$

$$V_{MAX} = 5 \log cz - 3.175 (\pm 0.025) \sigma = 0.26 \text{ n} = 29, \quad (2)$$

$$I_{MAX} = 5 \log cz - 2.948 (\pm 0.029) \sigma = 0.19 \text{ n} = 25. \quad (3)$$

Note that the quoted dispersion is the simple *rms* deviation of the points about the fit.

The most obvious property of these diagrams is that the dispersion is greatest for the nearest SNe. As pointed out in Paper IV, this property would be expected if the scatter were due primarily to the peculiar motions of the host galaxies. This would require that the galaxies possess peculiar motions with respect to the pure Hubble flow considerably in excess of the value of 600 km s^{-1} assumed in the horizontal error bars plotted in Figure 1. If we interpret

¹ Since the K terms for SNe Ia in the I band are not available in the literature we calculated these corrections based on our own spectroscopic observations of SNe Ia gathered at CTIO, following the same precepts described by Hamuy *et al.* (1993b).

the entire scatter in the V data in this figure as due to peculiar velocities, the *rms* velocity scatter would be $< (v_{CMB} - v_{Hubbleflow})^2 >^{1/2} = 1420 \text{ km s}^{-1}$. This value is dominated by large residuals at higher redshift; however, if we restrict the sample to the 11 galaxies within $10,000 \text{ km s}^{-1}$, the *rms* residual velocity is still 1050 km s^{-1} . These values are considerably in excess of measurements of the cosmic velocity dispersion. For example, Marzke *et al.* (1995) measure pairwise velocity differences from the CfA2 and Southern Sky Redshift Survey ranging between $299 \pm 99 \text{ km s}^{-1}$ and $540 \pm 180 \text{ km s}^{-1}$; the larger values are derived when dense virialized systems are included in the analysis. Since the SN found in the Calán/Tololo sample avoid rich Abell clusters and the scatter in the Hubble diagram derived above are still 3σ in excess of these larger values for pairwise velocities, it is extremely unlikely that a dominant portion of the observed scatter arises from peculiar motions.

Dust in the parent galaxies probably also contributes to the observed dispersion in the Hubble diagrams. Indeed, Table 1 shows that Na I D interstellar lines were detected in the spectra of a few of the SNe. In order to examine this alternative, we plot in Figure 2 the absolute magnitudes of the Calán/Tololo SNe as a function of the $B_{MAX}-V_{MAX}$ color. Plotted for comparison in the same figure are the Galactic reddening vectors (with slopes of 4.1 in B, 3.1 in V, and 1.85 in I) corresponding to a color excess of $E(B-V)=0.2$. We see that 26 of the 29 SNe lie in a well-defined clump centered on $B_{MAX}-V_{MAX} \sim 0.0$. Of the 3 outliers, SN 1992K is a SN 1991bg-like event whose very red color and low luminosity is almost certainly intrinsic (see Paper III). The spectrum of SN 1993H showed weak Na I D absorption (see Table 1), and so its red color may be evidence of significant dust extinction. However, the maximum-light spectrum of this object also showed Ti II absorption, similar in strength to that observed in the fast-declining SN 1986G (Phillips *et al.* 1987), which may indicate that the red color of this SN was at least partly intrinsic (see Nugent *et al.* 1995). In the case of SN 1990Y, the one spectrum available to us is of such low signal-to-noise that we can only place an uninteresting upper limit of 4 \AA on the equivalent width of any possible absorption due to the host galaxy. Hence, we cannot say whether the red color of this SN was intrinsic or due to dust extinction. The mean color of the remaining 26 SNe is $B_{MAX}-V_{MAX} = 0.03$, with an *rms* dispersion of only 0.06 mag. If this dispersion were entirely due to dust extinction in the host galaxies, it could account for as much as 0.25^m of the dispersion in the B Hubble diagram, 0.19^m in V, and 0.11^m in I. However, it is likely that at least part of the observed dispersion in color is intrinsic (e.g., SNe 1992bc versus 1992bo; Paper II) which, coincidentally, appears to run in the same direction as the reddening vectors. Although sorting out these two different possibilities –dust reddening versus an intrinsic color spread– is made difficult by the similar effects they display in a diagram like Fig. 2, we conclude that dust extinction in the parent galaxies is generally small, and cannot explain all of the observed dispersion in the Hubble diagrams.

As shown in Paper V, the major source of the dispersion in the Hubble diagrams in Figure 1 is an intrinsic spread in the peak luminosities of SNe Ia. Fortunately, as shown by Phillips (1993) and confirmed in Paper V (and also in a preliminary way in Paper IV), the absolute magnitudes at maximum light are strongly correlated with the initial decline rate of the B light curve. The sense of this correlation is that the most luminous SNe Ia display the slowest decline

rates. In Figure 1 of Paper V, the absolute magnitudes of the Calán/Tololo SNe are plotted as a function of the decline rate parameter $\Delta m_{15}(B)$. Excluding the 3 events (SNe 1990Y, 1992K, and 1993H) in the sample with $B_{\text{MAX}} - V_{\text{MAX}} > 0.2$, linear least-square fits to the data for the 26 remaining SNe yield slopes of 0.784 ± 0.182 in B, 0.707 ± 0.150 in V and 0.575 ± 0.178 in I. We shall use these relations in Sec. 4 to correct the Hubble diagrams for this effect.

A magnitude limited SNe search such as the Calán/Tololo survey is susceptible to variety of possible selection effects. Lower luminosity events will be increasingly difficult to find at larger redshifts, leading to classical Malmquist bias. In order to study this effect, we plot in Figure 3 the absolute BVI magnitudes of the Calán/Tololo SNe as a function of redshift. The most distant SNe ($\log cz > 4$) are not significantly brighter than the nearby sample, although it is clear that the faintest of the nearby SNe are not found in the distant sample. Indeed, the mean values for the nearest 11 SNe are slightly brighter than the distant sample of 18 ($M_{\text{MAX}}^B = -19.08 \pm 0.17$ for the nearby sample vs. -19.04 ± 0.06 for the distant SNe.) The major effect seen in Figure 3 is the larger scatter at lower redshifts. Malmquist bias may, however, affect the *slope* of the absolute magnitude-decline rate relation. In Paper V we found that the slope obtained for a nearby sample of SNe Ia with Cepheid, Surface Brightness Fluctuations, or Planetary Nebula Luminosity Function distances appeared to be steeper than the slope derived for the Calán/Tololo sample. We note that the four intrinsically-faintest SNe in the nearby sample would not have been discovered over most of the volume surveyed by the Calán/Tololo search, and thus the slopes obtained for the Calán/Tololo sample could be biased to flatter values.

A puzzling aspect of the sample which contributes to the scatter in this figure is that SNe hosted by spiral galaxies, which are the most luminous events of our sample (see Paper V), are preferentially found in the nearer sample. This apparent selection effect can be appreciated more clearly in the upper half of Figure 4 which shows the morphological types of the host galaxies of the Calán/Tololo SNe Ia (separated into basic categories of spirals and nonspirals) plotted as a function of redshift. Clearly the ratio of spirals/nonspirals is significantly higher in the nearby sample ($\log cz < 4$) than in the more distant group ($\log cz > 4$). In the lower half of Figure 4 we show another representation of this effect in a plot of $\Delta m_{15}(B)$ vs redshift. In the nearby sample we find three of the four largest values of $\Delta m_{15}(B)$, as might be expected from a Malmquist effect, since these are the fainter SNe. But we also find the four smallest values of $\Delta m_{15}(B)$ in this nearby sample, representing the brightest SNe. Thus the overall effect is to produce a large scatter in the Hubble diagram for nearby SNe.

As briefly discussed in Paper IV, there are several possible causes for this effect. It could be that the SNe in spiral galaxies occur preferentially near the central parts of the host galaxies or near spiral arms, posing increasing difficulties to their discovery at larger redshifts in a photographic search. There may also have been a bias in the survey to avoid nearby clusters (e.g., Virgo or Fornax) thus preferentially sampling the spiral rich field nearby; at larger distances rich clusters might not have been avoided, thus giving the observed morphological signal. While these are plausible explanations, the definitive cause of this rather unusual sample effect is still unclear. Whatever the exact cause, it appears that the derivation of the Hubble constant will

not be greatly affected by this somewhat bizarre sample effect because we correct for the dependence of absolute magnitude on $\Delta m_{15}(B)$. We caution, however, that attempts to derive the SNe Ia luminosity function from these data clearly *would* be affected, and the selection effects warrant more careful consideration.

4 Discussion

4.1 The corrected Hubble diagrams

The existence of the absolute magnitude-decline rate relation allows us to correct the apparent magnitudes of the Calán/Tololo SNe and reanalyze the corresponding Hubble diagrams. In keeping with Paper V, we shall limit the sample to the 26 events with $B_{MAX} - V_{MAX} \leq 0.20$.² As mentioned in Sec. 3 there is little room for significant extinction in the parent galaxies of this subsample of 26 events. Linear regression fits to the data for this subsample (ignoring for the moment the absolute magnitude-decline rate dependence) give the following zero points and dispersions:

$$B_{MAX} = 5 \log cz - 3.177 (\pm 0.029) \quad \sigma = 0.24 \quad n = 26, \quad (4)$$

$$V_{MAX} = 5 \log cz - 3.188 (\pm 0.026) \quad \sigma = 0.22 \quad n = 26, \quad (5)$$

$$I_{MAX} = 5 \log cz - 2.958 (\pm 0.030) \quad \sigma = 0.19 \quad n = 22. \quad (6)$$

The upper half of Figure 5 shows the V Hubble diagram for this subsample of 26 SNe. Excluding the 3 reddest events has helped to decrease the dispersion [cf. Equations. (1)–(3)], especially in the B band (0.24^m versus 0.38^m for the full sample). The effect in I, on the other hand, is negligible.

A more dramatic decrease in the dispersion of the Hubble diagrams is obtained by correcting for the peak luminosity-decline rate relation. Adopting the slopes derived in Paper V from the same sample of 26 Calán/Tololo SNe Ia, we obtain:

$$B_{MAX} - 0.784(\pm 0.182) [\Delta m_{15}(B) - 1.1] = 5 \log cz - 3.318 (\pm 0.035) \quad \sigma = 0.17 \quad n = 26, \quad (7)$$

$$V_{MAX} - 0.707(\pm 0.150) [\Delta m_{15}(B) - 1.1] = 5 \log cz - 3.329 (\pm 0.031) \quad \sigma = 0.14 \quad n = 26, \quad (8)$$

²A color cutoff (at $B_{MAX} - V_{MAX} < 0.25$) as an objective criteria to exclude heavily-reddened or intrinsically low-luminosity events has been proposed by Vaughan *et al.* (1995).

$$I_{MAX} - 0.575(\pm 0.178) [\Delta m_{15}(B) - 1.1] = 5 \log cz - 3.057 (\pm 0.035) \sigma = 0.13 \text{ n} = 22. \quad (9)$$

The second term on the left of these equations corrects the observed magnitudes of each SN to the equivalent magnitudes of an event with $\Delta m_{15}(B) = 1.1$ mag. The lower half of Figure 5 shows the corrected V Hubble diagram. Application of the peak magnitude-decline rate relation has reduced the scatter in this diagram to a level of 0.14^m which, as the value of the reduced χ^2 indicates, is now entirely consistent with the assumed errors. The reduction of σ by approximately a factor of 1.5 allows SNe Ia to be used as excellent distance indicators (with precisions in relative distances $\sim 7\text{-}10\%$). If we, again, interpret this scatter as being entirely due to peculiar velocities, the 11 nearest objects imply an rms velocity of 550 km s^{-1} . A more detailed analysis of the velocity field based on these data will be given in a separate paper (Suntzeff *et al.* 1996a).

We can test the sensitivity of these results to dust extinction in the host galaxies by restricting the sample even further to those objects for which we have been able to place an upper limit to the equivalent width of the Na I D interstellar lines $\leq 0.5 \text{ \AA}$. For gas typical of that found in the disk of our own Galaxy, such a limit corresponds to color excesses $E(B-V) \lesssim 0.1$. For the 15 SNe meeting this condition (90O, 90af, 91S, 91ag, 92J, 92ae, 92al, 92bc, 92bg, 92bh, 92bk, 92bl, 92bo, 93B, 93O), the zero points of the corrected Hubble diagrams prove to be -3.318 ± 0.046 in B, -3.324 ± 0.041 in V, and -3.039 ± 0.046 in I, which are insignificantly different than the zero points obtained from the 26 SNe.

4.2 The Hubble constant

Recently, Sandage and collaborators have measured Cepheid distances to the host galaxies of six nearby SNe Ia (SN 1937C in IC 4182, SNe 1895B and 1972E in NGC 5253, SN 1981B in NGC 4536, SN 1960F in NGC 4496, and SN 1990N in NGC 4639) with the aim to calibrate the Hubble diagram of the distant SNe Ia (Saha *et al.* 1994, 1995, 1996; Sandage *et al.* 1996). From these SNe, these authors obtained $H_0(B) = 56 \pm 4 \text{ km s}^{-1} \text{ Mpc}^{-1}$ and $H_0(V) = 58 \pm 4 \text{ km s}^{-1} \text{ Mpc}^{-1}$ (Sandage *et al.* 1996). Since these values were calculated without including corrections for the peak luminosity-decline rate relation, a reexamination of the Hubble constant based on the Calán/Tololo SNe would seem in order.

Owing to the poor quality of the light curves of SNe 1895B and 1960F (Schaefer 1995, 1996), we are unable to derive a precise estimate of the decline rate parameter $\Delta m_{15}(B)$. Hence, these two events are not considered in the remainder of this discussion. Although adequate photometry is available for SNe 1937C and 1972E, neither was observed at maximum light, so we must use the same χ^2 -minimizing template-fitting technique employed for the Calán/Tololo SNe to estimate their peak magnitudes and decline rates. SNe 1981B and 1990N, on the other hand, have well-sampled light curves with coverage beginning before maximum light so that the peak magnitudes and decline rates can be directly measured from the light curves. To

convert these values into absolute magnitudes, we assumed the *true* Cepheid distance moduli measured by Sandage and collaborators and the color excesses $E(B-V)$ from Burstein & Heiles (1984) for interstellar dust in our own galaxy. With this approach we wish to make the nearby sample reflect the properties of the distant sample for which we have not attempted to correct for possible obscuration in the host galaxies. Note that the mean $B_{MAX}-V_{MAX}$ color, corrected for foreground extinction, of the four calibrating SNe is 0.01 ± 0.07 (see Table 2), which is very close to the mean observed color of 0.03 ± 0.06 of the subsample of 26 Calán/Tololo events.

The relevant data for these four SNe with Cepheid distances are listed in Table 2 in the following format:

Column (1): SN name.

Column (2): the name of the host galaxy.

Column (3): the host galaxy morphology following the scheme in the Hubble Atlas of Galaxies (Sandage 1961).

Column (4): the true distance modulus of the host galaxy.

Column (5): references to the distance modulus given in column (4).

Column (6), (7) and (8): the apparent B, V, and I peak magnitudes of the SN as determined from the light curves. Note that the peak magnitudes that we derived for SN 1937C are brighter by 0.14^m in B and 0.18^m in V than those found by Pierce and Jacoby (1995). This difference is ascribed to the different techniques of fitting the light curve templates to the data.

Column (9): the decline rate parameter $\Delta m_{15}(B)$.

Column (10): the color excess $E(B-V)$ from Burstein & Heiles (1984) for interstellar dust in our own galaxy.

Column (11), (12) and (13): the absolute B, V, and I peak magnitudes of the SN calculated from the apparent magnitudes, the distance modulus of the host galaxy, and the assumed color excess. A standard Galactic reddening law was assumed to convert the color excess to the extinction in the B, V, and I bands. The error estimates include uncertainties from the apparent magnitude, distance modulus, and reddening.

Column (14): references to the SN photometry.

The value of the Hubble constant can be determined from the corrected Hubble diagrams of the Calán/Tololo SNe along with the absolute magnitudes of the 4 calibrating SNe, suitably corrected for their decline rates. From the corrected Hubble relations [Eqs. 7-9] we have,

$$\log H_0(B) = 0.2\{M_{MAX}^B - 0.784(\pm 0.182) [\Delta m_{15}(B) - 1.1] + 28.318(\pm 0.035)\}, \quad (10)$$

$$\log H_0(V) = 0.2\{M_{MAX}^V - 0.707(\pm 0.150) [\Delta m_{15}(B) - 1.1] + 28.329(\pm 0.031)\}, \quad (11)$$

$$\log H_0(I) = 0.2\{M_{MAX}^I - 0.575(\pm 0.178) [\Delta m_{15}(B) - 1.1] + 28.057(\pm 0.035)\}. \quad (12)$$

Table 3 summarizes our calculations for the individual calibrators. In columns (2)-(4) we give the absolute B, V, and I peak magnitudes of the individual SNe *corrected for the peak luminosity-decline rate relation*, where the error estimates include uncertainties from the apparent magnitude, foreground reddening, distance modulus, decline rate, and the slope of the absolute magnitude-decline rate relationship. In columns (5)-(7) we give the corresponding values of the Hubble constant obtained from Eqs. (10)-(12). The errors in H_0 include uncertainties in the (corrected) absolute magnitudes, the zero point of the Hubble diagram, and the observed scatter of the individual SNe in the corrected Hubble diagram (0.17^m in B, 0.14^m in V, and 0.13^m in I). In Table 4 we summarize the error budget of our calculations of the Hubble constant in the V filter for an individual SN (1972E). Weighted averages in B, V, and I of the absolute magnitudes and the values of the Hubble constant for the 4 calibrating SNe are given in the bottom line of Table 3.

Averaging the values of the Hubble constant for the three colors gives:

$$H_0 = 63.1 \pm 3.4 \text{ (internal)} \pm 2.9 \text{ (external)} \text{ km s}^{-1} \text{ Mpc}^{-1} .$$

Since the errors in the individual values of H_0 from B, V, and I are not all independent, we adopt an error for the mean which is the smallest of the uncertainties of the individual single-color determinations. The true internal error is probably smaller than this conservative estimate. The external error is the uncertainty in the zero point of the Cepheid calibration (assumed to be $\pm 0.10^m$). The resulting dispersion of $\sigma = 0.5 \text{ km s}^{-1} \text{ Mpc}^{-1}$ shows the good agreement among all three determinations of the Hubble constant.

Note that these values of H_0 are in excellent agreement with the preliminary results published in Paper IV from the 13 Calán/Tololo SNe, namely, $H_0(\text{B}) = 62 \pm 11 \text{ km s}^{-1} \text{ Mpc}^{-1}$ and $H_0(\text{V}) = 63 \pm 8 \text{ km s}^{-1} \text{ Mpc}^{-1}$.

Of the four calibrators, it could be argued that SNe 1981B and 1990N should be given more weight than SNe 1937C and 1972E for several reasons. First of all, the maximum light magnitudes of 1981B and 1990N were directly observed, whereas we had to estimate those of 1937C and 1972E through template fitting. Secondly, and probably more important, SNe 1981B and 1990N both had decline rates of $\Delta m_{15}(\text{B}) \sim 1.1$, which is the reference value we have employed because it is “typical” for type Ia events like those discovered in the Calán/Tololo survey (see the lower half of Figure 4, or Figure 2 of Paper V). SNe 1937C and 1972E, on the other hand, were slow-declining events ($\Delta m_{15}(\text{B}) \sim 0.9$), and therefore fall at the extreme end of the peak luminosity-decline rate relation (see Figure 2 of Paper V). Use of 1981B and 1990N therefore minimizes the effect of uncertainties or biases in the slopes of the absolute magnitude-decline rate relations. A weighted average of the absolute magnitudes of Table 3 for SNe 1981B and 1990N alone yields a Hubble constant:

$$H_0 = 66.9 \pm 5.2 \text{ (internal)} \pm 3.1 \text{ (external)} \text{ km s}^{-1} \text{ Mpc}^{-1} .$$

If we ignore the peak luminosity-decline rate relation, the four calibrating SNe Ia give $H_0(\text{B}) = 55.9 \pm 3.9 \text{ km s}^{-1} \text{ Mpc}^{-1}$, $H_0(\text{V}) = 56.4 \pm 3.7 \text{ km s}^{-1} \text{ Mpc}^{-1}$, and $H_0(\text{I}) = 57.1 \pm 5.5 \text{ km s}^{-1} \text{ Mpc}^{-1}$, which are in close agreement with the results of Sandage *et al.* (1996). This similarity is not surprising since we are using their Cepheid calibrations and the Hubble diagram they use (Tammann & Sandage 1995) is heavily weighted by the inclusion of seven distant Calán/Tololo SNe from Paper IV. If, however, we use only SNe 1981B and 1990N as the calibrators for the same reasons given in the previous paragraph, these values increase to $H_0(\text{B}) = 63.8 \pm 6.5 \text{ km s}^{-1} \text{ Mpc}^{-1}$, $H_0(\text{V}) = 62.3 \pm 5.9 \text{ km s}^{-1} \text{ Mpc}^{-1}$, and $H_0(\text{I}) = 60.5 \pm 8.5 \text{ km s}^{-1} \text{ Mpc}^{-1}$. Note that the latter values are now very close to the Hubble constant that we derive when we correct for the absolute magnitude-decline relationship. *This is because SNe 1981B and 1990N are much more representative (in terms of both decline rate and luminosity) of the “average” SNe Ia which are included in the Hubble diagrams of both the present paper and that of Tammann & Sandage (1995).* As we have shown in Paper V, there is now strong evidence that galaxies with younger stellar population (spirals and irregulars) appear to host the slowest-declining, and therefore most luminous SNe I. Hence, the use of Pop I objects such as Cepheids to calibrate the zero point of the SNe Ia Hubble diagram can easily bias the results toward luminous SNe Ia, *unless the absolute magnitude-decline relation is taken into account.*

4.3 The Recession Velocities of the Virgo and Fornax Clusters

Freedman *et al.* (1994) have used HST to measure a Cepheid distance to M100 of $17.1 \pm 2 \text{ Mpc}$ ($\mu = 31.16 \pm 0.20$)³. Based on this distance and an assumed cosmic recession velocity of $1,404 \pm 80 \text{ km s}^{-1}$, this group found a value of $H_0 = 82 \pm 17 \text{ km s}^{-1} \text{ Mpc}^{-1}$. Whether the Freedman *et al.* choice of $1,404 \text{ km s}^{-1}$ is correct or not rests on the adopted corrections for the peculiar velocity of Virgo. Estimates of the extragalactic distance scale based on the Virgo cluster suffer from large uncertainties due to the possible peculiar velocity of the cluster and cluster depth. On the other hand, our method of using distant SNe Ia is not affected by this problem since the peculiar motions of the Calán/Tololo SNe are a small fraction of their redshifts.

We can use our observed Hubble diagram, combined with historical observations of the SNe Ia in the Virgo and Fornax clusters to predict their recession velocities and relative distances. An earlier attempt to derive the Virgo distance in this manner was made by Leibundgut & Tammann (1990) and Leibundgut & Pinto (1992); more recent photometry and the peak magnitude-decline rate relation indicate that a rediscussion of this issue is worthwhile. In Table 5 we summarize the Virgo and Fornax SNe with modern photometry. The scatter in the photographic light curves for SN 1984A limits our ability to measure a precise value of $\Delta m_{15}(\text{B})$

³ A recent reanalysis of these data by the same group gives a distance of $16.1 \pm 1.3 \text{ Mpc}$, or $\mu = 31.04 \pm 0.17$ (Ferrarese *et al.* 1996).

for this event; we shall assume that this SN has the fiducial decline rate value of 1.10 (± 0.10).

Excluding the peculiar event SN 1991bg, we find $\langle B \rangle = 12.16^m \pm 0.20$, $\langle V \rangle = 12.07^m \pm 0.20$, and $\langle I \rangle = 12.23^m \pm 0.39$ for Virgo and $\langle B \rangle = 12.53^m \pm 0.04$, $\langle V \rangle = 12.50^m \pm 0.05$, and $\langle I \rangle = 12.75^m \pm 0.05$ for Fornax. The results of correcting the peak magnitudes of the individual SNe for the magnitude-decline rate relation are shown in Table 6. Here the quoted errors for the individual corrected magnitudes include the photometric and decline rate errors given in Table 5, the errors in the slopes that we have fitted to the absolute magnitude-decline rate relation, and the uncertainty in the observed scatter of the individual SNe in the Hubble diagrams (0.17^m in B, 0.14^m in V, and 0.13^m in I). Note that the average $\Delta m_{15}(B)$ for the Virgo SNe is ~ 1.10 and therefore the mean corrected magnitudes (also shown in Table 6) are very similar to the mean observed magnitudes given above, while the faster decline rates of the two Fornax SNe act to make the corrected magnitudes somewhat brighter. We have not corrected for foreground reddening since the reddening values are zero for both Virgo and Fornax, based on the maps of Burstein and Heiles (1982). Regarding possible obscuration in the host galaxies, note that the mean color of the five Virgo SNe ($\langle B-V \rangle = 0.09 \pm 0.10(rms)$) and the two Fornax SNe ($\langle B-V \rangle = 0.03 \pm 0.02(rms)$) are very close to the mean color of the Calán/Tololo SNe ($\langle B-V \rangle = 0.03 \pm 0.06(rms)$). Also, all of the Virgo and Fornax SNe considered here have $B-V \leq 0.20$ which is the color cutoff that we use as an objective criteria to exclude heavily reddened events in the Calán/Tololo SNe. Hence, we believe that host galaxy reddening in the Fornax and Virgo SNe is not significantly different than that in the distant sample.

Table 6 shows that, in all three colors, the standard deviation of the corrected magnitudes for the Virgo SNe is greater than the errors in the individual magnitudes. A likely source for this additional dispersion is the significant depth of the cluster, estimated by Freedman *et al.* (1994) to be $\pm 0.35^m$ and also apparent in the few Cepheid distances of Virgo cluster galaxies obtained to date (Sandage *et al.* 1996). On the other hand, the standard deviation of the corrected magnitudes of the two Fornax SNe is much less than the errors in the individual magnitudes. Although we expect that depth effects for Fornax will be small due to the compact nature of the cluster, the extremely close agreement in the corrected magnitudes of the two SNe must be a fortuitous consequence of small number statistics. Hence, we shall use the individual errors in the corrected magnitudes to estimate realistic errors in the mean corrected magnitudes for Fornax, adopting 0.13^m ($0.19^m/\sqrt{2}$) in B, 0.11^m ($0.16^m/\sqrt{2}$) in V, and 0.10^m ($0.15^m/\sqrt{2}$) in I.

If we now apply equations (7), (8) and (9), we derive the cosmic recession velocities shown in Table 6. Restricting ourselves to the B and V results for Virgo, for which there is data for all five SNe, the resulting mean velocity for Virgo is $1,223 \text{ km s}^{-1}$, to which we conservatively assign an error ⁴ of $\pm 115 \text{ km s}^{-1}$. The corresponding value for Fornax is $1,342 \pm 70 \text{ km s}^{-1}$, where we have used the results in all three colors.

⁴The errors in the individual recession velocities derived from B and V are at least partially correlated (e.g., due to the effect of cluster depth), and so we adopt an error for the mean which is typical of the uncertainties in the individual single-color determinations. The true error is probably somewhat less than this estimate.

In Table 7 we show a comparison of these predicted v_{CMB} values with recent results from the literature. The predicted value for Fornax agrees well with the measured velocities. The situation for Virgo is more complex, since there is a wide range of estimates for the correct velocity. Based on the cosmic recession velocity of Virgo of $1,223 \text{ km s}^{-1}$ estimated here we can derive our infall velocity into Virgo. Adopting the observed heliocentric cluster velocity of $1,050 \pm 35 \text{ km s}^{-1}$ from Bingelli *et al.* (1993) and a correction of -107 km s^{-1} to the Local Group center derived from the Galactic coordinates ($l = 284^\circ$, $b = 74^\circ$) and the transformation vector given by Lynden-Bell & Lahav (1988), we infer an infall of $280 \pm 120 \text{ km s}^{-1}$. This value is consistent with the Aaronson *et al.* (1982) result of $331 \pm 41 \text{ km s}^{-1}$ and more recent determinations (e.g., Jerjen & Tammann 1993, Bureau *et al.* 1996), although clearly a larger sample of SNe are needed to improve the significance of the result. Note also that there is still disagreement over the correct value of the heliocentric velocity of Virgo; if we use Huchra's (1988) preferred value of $1,150 \pm 51 \text{ km s}^{-1}$, an infall velocity of $180 \pm 126 \text{ km s}^{-1}$ is implied.

From these corrected mean magnitudes we can also derive relative distance moduli. We find $\Delta\mu(\text{B})=0.15^m \pm 0.24^m$ and $\Delta\mu(\text{V})=0.23^m \pm 0.23^m$ for a combined estimate of $\Delta\mu=0.19^m \pm 0.23^m$. This lies about $1\text{-}\sigma$ from a recent result from the I-band Tully–Fisher relation of $\Delta\mu=-0.06\pm 0.15$ (Bureau *et al.* 1996). Again, the accuracy of the determination will improve considerably when more SNe are discovered in either cluster.

Finally if we assume the average absolute magnitudes corrected for the peak luminosity–decline rate relation of the four nearby calibrators given at the bottom of Table 3, we can make the following predictions:

- The true distance modulus of Virgo is 31.41 ± 0.22 . Therefore, M100 ($\mu=31.04 \pm 0.17$) is most likely on the near side of the cluster.
- The distance modulus of the Fornax cluster is 31.60 ± 0.15 .

Due to the problem of the intrinsic depth of the Virgo cluster (assumed by Freedman *et al.* to be $\pm 0.35^m$ in distance modulus), Cepheid distances for a number of spirals will be needed before the first prediction can be verified. Hence, the easiest prediction to test is, in fact, the distance to the Fornax cluster since this cluster is relatively nearby and has a much smaller depth ($<0.15^m$). A recent determination of the Cepheid distance to NGC 1365 in Fornax, yields a distance modulus of $31.30^m \pm 0.23^m$ (Freedman 1996), in reasonable agreement with the above determination.

5 Conclusions

1) The main goal of the Calán/Tololo survey which we initiated in 1990 was to address the question of how reliable are Type Ia SNe as extragalactic standard candles. The Calán/Tololo

database has shown that the Hubble diagrams of SNe Ia are characterized by significant dispersions that range between $\sim 0.4^m$ in B and $\sim 0.2^m$ in I. Thus, SNe Ia are far from being perfect standard candles. Nevertheless, the relatively small dispersion observed in I is encouraging, and suggests that future work should make more use of this band.

2) The Calán/Tololo database has confirmed the finding of Phillips (1993) from a group of nearby SNe Ia that the luminosities of these events are correlated with the initial decline rates of their light curves (see Paper V), although this effect seems to be less pronounced than in the original sample studied by Phillips. Application of the peak luminosity-decline rate relationship results in a significant decrease in the scatter in the BVI Hubble diagrams to levels 0.17^m - 0.13^m . Thus, after correcting the apparent magnitudes for the decline rates, SNe Ia can be used to derive relative distances with precisions ~ 7 - 10% .

3) Using published Cepheid distances to SNe 1937C, 1972E, 1981B, and 1990N to calibrate the zero point of the “corrected” BVI Hubble diagrams we obtain a value for the Hubble constant of $H_0=63.1\pm 3.4$ (internal) ± 2.9 (external) $\text{km s}^{-1} \text{Mpc}^{-1}$. The implication of ignoring the peak luminosity-decline rate relation is to underestimate the Hubble constant by a factor ~ 10 - 15% .

4) Using the inertial reference frame of the distant SNe Ia, and the “corrected” apparent magnitudes of the five best-observed SNe Ia in the Virgo cluster and two SNe Ia in the Fornax cluster, we predict the Hubble flow at Virgo of $1,223\pm 115 \text{ km s}^{-1}$ and $1,342\pm 70 \text{ km s}^{-1}$ for Fornax. The “corrected” magnitudes also imply a relative distance modulus of $\Delta\mu(\text{Fornax-Virgo}) = 0.19^m\pm 0.23^m$.

5) Given the high intrinsic brightness, SNe Ia provide a unique tool for measuring the distances to very distant galaxies and, thus, the deceleration parameter q_0 (e.g., see Perlmutter *et al.* 1995). This will be, of course, a challenging task since a large number of events at redshifts of 0.3-0.5 will have to be observed. Furthermore, the need to measure the decline rate of such objects will require large telescopes. With a collective effort, however, such a goal appears achievable nowadays.

Acknowledgments

We are extremely grateful to the large number of CTIO visiting astronomers and CTIO staff members who gathered data for this project. We also thank Gary Schmidt and George Jacoby for useful discussions. This paper has been possible thanks to grant 92/0312 from Fondo Nacional de Ciencias y Tecnología (FONDECYT-Chile). MH acknowledges support provided for this work by the National Science Foundation through grant number GF-1002-96 from the

Association of Universities for Research in Astronomy, Inc., under NSF Cooperative Agreement No. AST-8947990 and from Fundación Andes under project C-12984. JM acknowledges support by Cátedra Presidencial 1996/97.

References

- Aaronson, M., Huchra, J., Mould, J., Schechter, P.L., & Tully, R.B. 1982, ApJ, 258, 64
- Barbon, R., Ciatti, F., & Rosino, L. 1982, A&A, 116, 35
- Barbon, R., Iijima, T., & Rosino, L. 1989, A&A, 220, 83
- Binggelli, B., Popescu, C.C., & Tammann, G.A. 1993, A&AS, 98, 275
- Bureau, M., Mould, J.R., & Stavely-Smith, L. 1996, ApJ, 463, 60
- Burstein, D., & Heiles, C. 1982, AJ, 87, 1165
- Burstein, D., & Heiles, C. 1984, ApJS, 54, 33
- Buta, R.J., & Turner, A. 1983, PASP, 95, 72
- Ferrarese, L., *et al.* 1996, ApJ, 464, 568
- Filippenko, A.V., *et al.* 1992, AJ, 104, 1543
- Freedman, W.L., *et al.* 1994, Nature, 371, 757
- Freedman, W.L. 1996, in proceedings of *The Extragalactic Distance Scale*, STScI Spring meeting, ed. M. Livio, in preparation
- Hamuy, M., Phillips, M.M., Maza, J., Wischnjewsky, M., Uomoto, A., Landolt, A.U., & Khatwani, R. 1991, AJ, 102, 208
- Hamuy, M., *et al.* 1993a, AJ, 106, 2392 (Paper I)
- Hamuy, M., Phillips, M.M., Wells, L.A., & Maza, J. 1993b, PASP, 105, 787
- Hamuy, M., *et al.* 1994, AJ, 108, 2226 (Paper III)
- Hamuy, M., Phillips, M.M., Maza, J., Suntzeff, N.B., Schommer, R.A., & Avilés, R. 1995, AJ, 109, 1 (Paper IV)
- Hamuy, M., Phillips, M.M., Schommer, R.A., Suntzeff, N.B., Maza, J., & Avilés, R. 1996a, AJ, this volume (Paper V)
- Hamuy, M., *et al.* 1996b, AJ, this volume (Paper VII)

- Hamuy, M., *et al.* 1996c, AJ, this volume (Paper VIII)
- Held, E.V., & Mould, J.R. 1994, AJ 107, 1307
- Huchra, J.P. 1988, in *The Extragalactic Distance Scale*, ASP Conference Series, Vol. 4, ed. S. van den Bergh & C.J. Pritchet (Provo: Brigham Young Univ. Print Services), 257
- Jerjen, H., & Tammann, G.A. 1993, A&A, 276, 1
- Kimeridze, G.N., & Tsvetkov, D.Y. 1986, Ap, 25, 513
- Leibundgut, B., & Tammann, G.A. 1990, A&A, 230, 81
- Leibundgut, B., & Pinto, P.A. 1992, ApJ, 401, 49
- Leibundgut, B., *et al.* 1993, AJ, 105, 301
- Lira, P. 1995, MS Thesis, Universidad de Chile.
- Lynden-Bell, D., & Lahav, O. 1988, in *Large-Scale Motions in the Universe* ed. V.C. Rubin & G.V. Coyne (Princeton: Princeton Univ. Press), 199
- Marzke, R. O., Geller, M. J., da Costa L. N., & Huchra, J. P., 1995, AJ, 110, 477
- Maza, J., Hamuy, M., Phillips, M.M., Suntzeff, N.B., & Avilés, R. 1994, ApJ, 424, L107 (Paper II)
- Nugent, P., Phillips, M., Baron, E., Branch, D., & Hauschildt, P. 1995, ApJ, 455, L147
- Perlmutter, S., *et al.* 1995, ApJ, 440, L41
- Phillips, M.M., *et al.* 1987, PASP, 99, 592
- Phillips, M.M. 1993, ApJ, 413, L105
- Phillips, M.M., & Eggen, O.J. 1996, in preparation
- Pierce, M.J., & Jacoby, G.H. 1995, AJ, 110, 2885
- Saha, A., Labhardt, L., Schwengeler, H., Macchetto, F.D., Panagia, N., Sandage, A., & Tammann, G.A. 1994, ApJ, 425, 14
- Saha, A., Sandage, A., Labhardt, L., Schwengeler, H., Tammann, G.A., Panagia, N., & Mac-

- chetto, F.D. 1995, ApJ, 438, 8
- Saha, A., Sandage, A., Labhardt, L., Tammann, G.A., Macchetto, F.D., & Panagia, N. 1996, ApJ, in press
- Sandage, A. 1961, *The Hubble Atlas of Galaxies* (Carnegie Institution of Washington, Washington DC)
- Sandage, A., Saha, A., Tammann, G.A., Labhardt, L., Panagia, N., & Macchetto, F.D. 1996, ApJ, 460, L15
- Schaefer, B.E. 1995, ApJ, 447, L13
- Schaefer, B.E. 1996, ApJ, 460, L19
- Smith, R.C., *et al.* 1996, in preparation
- Smoot, G.F., *et al.* 1992, ApJ, 396, L1
- Suntzeff, N.B. *et al.* 1996a, in preparation
- Suntzeff, N.B. *et al.* 1996b, in preparation
- Tammann, G.A., & Sandage, A. 1995, ApJ, 452, 16
- Tsvetkov, D.Y. 1982, SvAL, 8, 115
- Vaughan, T.E., Branch, D., Miller, D.L., & Perlmutter, S. 1995, ApJ, 439, 558

Figure Captions

Figure 1. The Hubble diagrams in B, V, and I for the 29 Calán/Tololo SNe Ia.

Figure 2. The absolute B, V, and I magnitudes of the Calán/Tololo sample of 29 SNe Ia, plotted as a function of their $B_{\text{MAX}} - V_{\text{MAX}}$ colors. The Galactic reddening vectors (with slopes of 4.1 in B, 3.1 in V, and 1.85 in I) corresponding to $E(B-V)=0.2$ are indicated.

Figure 3. The absolute B, V, and I magnitudes of the Calán/Tololo SNe Ia plotted as a function of redshift. The vertical line at $\log cz = 4$ ($10,000 \text{ km s}^{-1}$) illustrates the separation of the sample into two groups.

Figure 4. (top) The morphological types of their host galaxies of the Calán/Tololo SNe Ia plotted as a function of redshift. Note that the ratio of spirals/nonspirals is significantly higher in the nearby sample ($\log cz < 4$) than in the more distant group ($\log cz > 4$). (bottom) The decline rate ($\Delta m_{15}(B)$) plotted vs redshift. Note the wide spread in decline rates in the nearby sample, indicative of the full range of morphological types seen in the top panel.

Figure 5. (top panel) The Hubble diagram in V for the SNe Ia in the Calán/Tololo sample with $B_{\text{MAX}} - V_{\text{MAX}} \leq 0.20$. (bottom panel) The Hubble diagram for the same 26 events after correction for the peak luminosity-decline rate dependence.

Table 1. Colors and Magnitudes of the Calán/Tololo Supernovae Ia

(1)	(2)	(3)	(4)	(5)	(6)	(7)	(8)	(9)	(10)	(11)
SN	$\log(cz)$ CMB	B_{MAX}	V_{MAX}	I_{MAX}	$B_{MAX}-V_{MAX}$	M_{MAX}^B $+5\log(H_0/65)$	M_{MAX}^V $+5\log(H_0/65)$	M_{MAX}^I $+5\log(H_0/65)$	$\Delta m_{15}(B)$	EW(NaID) [Å]
90O	3.958(28)	16.32(10)	16.31(08)	16.70(09)	0.01(05)	-19.40(17)	-19.41(16)	-19.02(17)	0.96(10)	<0.2
90T	4.080(22)	17.16(21)	17.12(16)	17.35(15)	0.04(10)	-19.17(24)	-19.21(19)	-18.98(19)	1.15(10)	1.0
90Y	4.066(22)	17.70(21)	17.37(16)	17.61(15)	0.33(10)	-18.56(24)	-18.89(20)	-18.65(19)	1.13(10)	<4.0
90af	4.178(17)	17.87(07)	17.82(06)	—	0.05(03)	-18.95(11)	-19.00(11)	—	1.56(05)	<0.2
91S	4.223(16)	17.81(21)	17.77(16)	18.07(15)	0.04(10)	-19.24(22)	-19.28(18)	-18.98(17)	1.04(10)	<0.4
91U	3.992(28)	16.40(21)	16.34(16)	16.52(15)	0.06(10)	-19.49(25)	-19.55(21)	-19.37(20)	1.06(10)	0.8
91ag	3.616(63)	14.62(14)	14.54(15)	14.86(19)	0.08(05)	-19.40(35)	-19.48(35)	-19.16(37)	0.87(10)	0.0
92J	4.137(20)	17.70(21)	17.58(16)	17.84(15)	0.12(10)	-18.92(23)	-19.04(19)	-18.78(18)	1.56(10)	<0.2
92K	3.523(92)	15.83(21)	15.09(16)	14.94(15)	0.74(10)	-17.72(44)	-18.46(42)	-18.61(42)	1.93(10)	<0.2
92P	3.897(35)	16.08(07)	16.11(06)	16.39(06)	-0.03(03)	-19.34(18)	-19.31(18)	-19.03(18)	0.87(10)	1.2
92ae	4.351(12)	18.62(12)	18.51(08)	—	0.11(05)	-19.07(13)	-19.18(10)	—	1.28(10)	<0.5
92ag	3.891(36)	16.41(08)	16.28(07)	16.41(06)	0.13(05)	-18.98(19)	-19.11(18)	-18.98(18)	1.19(10)	1.1
92al	3.627(60)	14.60(07)	14.65(06)	14.94(06)	-0.05(03)	-19.47(32)	-19.42(31)	-19.13(31)	1.11(05)	<0.05
92aq	4.481(09)	19.45(09)	19.35(07)	19.77(09)	0.10(05)	-18.89(10)	-18.99(08)	-18.57(10)	1.46(10)	<1.1
92au	4.260(14)	18.21(21)	18.16(16)	18.41(15)	0.05(10)	-19.03(22)	-19.08(18)	-18.83(17)	1.49(10)	<1.3
92bc	3.774(44)	15.16(07)	15.24(06)	15.58(05)	-0.08(03)	-19.64(23)	-19.56(23)	-19.22(22)	0.87(05)	<0.2
92bg	4.030(25)	16.72(08)	16.76(07)	17.04(06)	-0.04(05)	-19.36(15)	-19.32(14)	-19.04(14)	1.15(10)	<0.3
92bh	4.131(20)	17.70(08)	17.62(06)	17.80(06)	0.08(05)	-18.89(13)	-18.97(11)	-18.79(11)	1.05(10)	<0.5
92bk	4.240(15)	18.11(10)	18.11(07)	18.31(06)	0.00(05)	-19.03(12)	-19.03(10)	-18.83(10)	1.57(10)	<0.4
92bl	4.110(20)	17.36(08)	17.36(07)	17.64(06)	0.00(05)	-19.13(13)	-19.13(12)	-18.85(12)	1.51(10)	<0.5
92bo	3.736(46)	15.86(07)	15.85(06)	15.97(05)	0.01(03)	-18.76(25)	-18.77(25)	-18.65(24)	1.69(05)	<0.2
92bp	4.374(11)	18.41(07)	18.46(06)	18.78(06)	-0.05(05)	-19.40(09)	-19.35(08)	-19.03(08)	1.32(10)	<1.1
92br	4.420(10)	19.38(17)	19.34(10)	—	0.04(05)	-18.66(18)	-18.70(11)	—	1.69(10)	<4.0
92bs	4.279(14)	18.37(09)	18.30(07)	—	0.07(05)	-18.96(11)	-19.03(10)	—	1.13(10)	<3.1
93B	4.326(13)	18.53(11)	18.41(09)	18.70(10)	0.12(05)	-19.04(13)	-19.16(11)	-18.87(12)	1.04(10)	<0.5
93H	3.872(37)	16.84(08)	16.61(06)	16.55(06)	0.23(05)	-18.45(19)	-18.68(19)	-18.74(19)	1.69(10)	1.2
93O	4.193(17)	17.67(07)	17.76(06)	17.99(06)	-0.09(03)	-19.23(11)	-19.14(10)	-18.91(10)	1.22(05)	<0.1
93ag	4.177(18)	17.72(08)	17.69(06)	18.01(06)	0.03(05)	-19.10(12)	-19.13(11)	-18.81(11)	1.32(10)	?
93ah	3.935(29)	16.33(21)	16.37(16)	16.68(15)	-0.04(10)	-19.28(26)	-19.24(22)	-18.93(21)	1.30(10)	?

Table 2. Nearby SNe Sample

(1)	(2)	(3)	(4)	(5)	(6)	(7)	(8)	(9)	(10)	(11)	(12)	(13)	(14)
SN	Host Galaxy	Morph. Type	Distance Modulus	Distance Modulus Ref ^a	B_{MAX}	V_{MAX}	I_{MAX}	$\Delta m_{15}(B)$	E(B-V)	M_{MAX}^B	M_{MAX}^V	M_{MAX}^I	Phot Ref ^b
1937C	IC 4182	S/Irr	28.36(09)	1	8.80(09)	8.82(11)	—	0.87(10)	0.00(02)	-19.56(15)	-19.54(16)		1
1972E	NGC 5253	Irr	27.97(07)	2	8.49(14)	8.49(15)	8.80(19)	0.87(10)	0.05(02)	-19.69(18)	-19.64(18)	-19.26(21)	2
1981B	NGC 4536	Sc	31.10(13)	3	12.03(03)	11.93(03)	—	1.10(05)	0.00(02)	-19.07(16)	-19.17(15)		3,4,5
1990N	NGC 4639	Sb	32.00(23)	4	12.74(03)	12.72(03)	12.95(05)	1.07(05)	0.00(02)	-19.26(25)	-19.28(24)	-19.05(24)	6

^aReferences.- ¹Saha *et al.* (1994); ²Saha *et al.* (1995); ³Saha *et al.* (1996); ⁴Sandage *et al.* (1996).

^bReferences.- ¹Pierce & Jacoby (1995); ²Phillips & Eggen (1996); ³Buta & Turner (1983); ⁴Barbon *et al.* (1982); ⁵Tsvetkov (1982); ⁶Lira (1995).

Table 3. Corrected Absolute Magnitudes and Values of H_0

(1)	(2)	(3)	(4)	(5)	(6)	(7)
SN	$M_{\text{MAX,corr}}^B$	$M_{\text{MAX,corr}}^V$	$M_{\text{MAX,corr}}^I$	$H_0(\text{B})$	$H_0(\text{V})$	$H_0(\text{I})$
1937C	-19.38(18)	-19.38(17)	—	61.3(7.0)	61.7(6.4)	
1972E	-19.50(20)	-19.47(19)	-19.13(22)	57.9(7.0)	59.1(6.6)	61.0(7.2)
1981B	-19.07(16)	-19.17(15)	—	70.7(7.7)	67.9(6.5)	
1990N	-19.24(25)	-19.26(24)	-19.03(24)	65.5(9.2)	65.2(8.5)	63.8(8.1)
Weighted						
Average	-19.28(10)	-19.31(09)	-19.08(16)	63.3(3.8)	63.3(3.4)	62.2(5.4)
	$\sigma=0.20$	$\sigma=0.14$	$\sigma=0.07$	$\sigma=5.6$	$\sigma=4.0$	$\sigma=2.0$

Notes:

$$M_{\text{MAX,corr}}^B = M_{\text{MAX}}^B - 0.784 [\Delta m_{15} - 1.1]$$

$$M_{\text{MAX,corr}}^V = M_{\text{MAX}}^V - 0.707 [\Delta m_{15} - 1.1]$$

$$M_{\text{MAX,corr}}^I = M_{\text{MAX}}^I - 0.575 [\Delta m_{15} - 1.1]$$

Table 4. Error Budget in the Calculation of $H_0(V)$

	Error Source	SN 1972E Error(mag)
1	Apparent V Magnitude	0.15^m
2	Reddening ($=3.1*\sigma_{E(B-V)}$)	0.06^m
3	Distance Modulus	0.07^m
4	Absolute V Magnitude ($=(1)+(2)+(3)$)	0.18^m
5	M_{MAX} vs Δm_{15} slope ($=0.15*[\Delta m_{15}-1.1]$)	0.03^m
6	Δm_{15} ($=0.10^m*0.707$)	0.07^m
7	Corrected Absolute V Magnitude ($=(4)+(5)+(6)$)	0.19^m
8	Zero Point of Hubble Diagram	0.031^m
9	Scatter of Hubble Diagram	0.14^m
	Total ($=(7)+(8)+(9)$)	0.24^m $=6.6 \text{ km s}^{-1} \text{ Mpc}^{-1}$

Table 5. SNe in Virgo and Fornax with Modern Photometry

(1)	(2)	(3)	(4)	(5)	(6)	(7)
SN	Host Galaxy	B_{obs}	V_{obs}	I_{obs}	$\Delta m_{15}(B)$	Photometry References
Virgo						
1981B	NGC 4536	12.03(03)	11.93(03)	—	1.10(05)	1,2,3
1984A	NGC 4419	12.50(10)	12.30(10)	—	—	4,5
1990N	NGC 4639	12.74(03)	12.72(03)	12.95(05)	1.07(05)	6
1991T	NGC 4527	11.69(03)	11.51(03)	11.62(03)	0.94(05)	6
1991bg	NGC 4374	14.76(10)	13.97(05)	13.51(05)	1.93(10)	7,8
1994D	NGC 4526	11.86(03)	11.90(03)	12.11(03)	1.32(05)	9
Fornax						
80N	NGC 1316	12.49(03)	12.44(03)	12.70(04)	1.28(04)	10
92A	NGC 1380	12.57(03)	12.55(03)	12.80(03)	1.47(05)	11

References.- ¹Buta & Turner (1983); ²Barbon *et al.* (1982); ³Tsvetkov (1982);
⁴Barbon *et al.* (1989); ⁵Kimeridze & Tsvetkov (1986); ⁶Lira (1995); ⁷Filippenko *et al.* (1992);
⁸Leibundgut *et al.* (1993); ⁹Smith *et al.* (1996); ¹⁰Hamuy *et al.* (1991); ¹¹Suntzeff *et al.* (1996b).

Table 6. Corrected Magnitudes for SNe in Virgo and Fornax

(1)	(2)	(3)	(4)
SN	B_{corr}	V_{corr}	I_{corr}
Virgo:			
1981B	12.03(18)	11.93(15)	—
1984A	12.50(21)	12.30(19)	—
1990N	12.76(18)	12.74(15)	12.97(14)
1991T	11.82(18)	11.62(15)	11.71(14)
1994D	11.69(18)	11.74(15)	11.98(14)
Average	12.16(20) $\sigma=0.46$	12.07(20) $\sigma=0.46$	12.22(38) $\sigma=0.66$
Velocity(CMB)	1,246(119) km s ⁻¹	1,200(114) km s ⁻¹	1,137(200) km s ⁻¹
Fornax:			
80N	12.35(18)	12.31(15)	12.60(14)
92A	12.28(19)	12.29(16)	12.59(15)
Average	12.31(03) $\sigma=0.05$	12.30(01) $\sigma=0.02$	12.59(01) $\sigma=0.01$
Velocity(CMB)	1,339(83) km s ⁻¹	1,337(69) km s ⁻¹	1,348(68) km s ⁻¹

Notes:

$$B_{corr} = B_{obs} - 0.784 [\Delta m_{15} - 1.1]$$

$$V_{corr} = V_{obs} - 0.707 [\Delta m_{15} - 1.1]$$

$$I_{corr} = I_{obs} - 0.575 [\Delta m_{15} - 1.1]$$

Table 7. Recessional Velocities of the Virgo and Fornax Clusters

Cluster	Predicted v_{CMB} [km s ⁻¹]	Previous Values [km s ⁻¹]	Reference
Virgo	1,223 ±115	1,179 1,404	Jerjen & Tammann 1993 Huchra 1988
Fornax	1,342 ±70	1,338 1,354	Jerjen & Tammann 1993 Held & Mould 1994

Calán/Tololo SNe Ia
Raw Hubble Diagrams

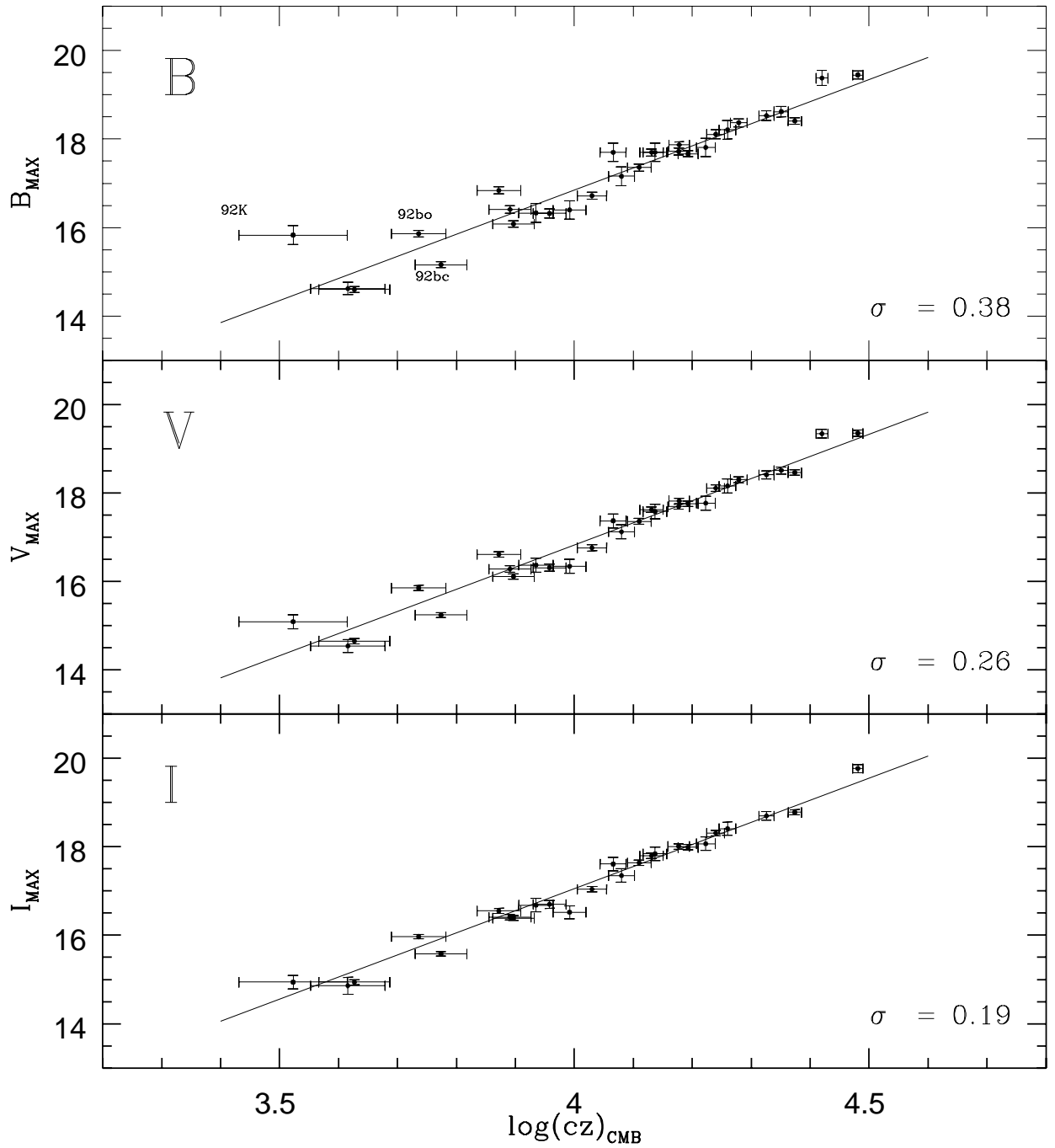


Figure 1: The Hubble diagrams in B, V, and I for the 29 Calán/Tololo SNe Ia.

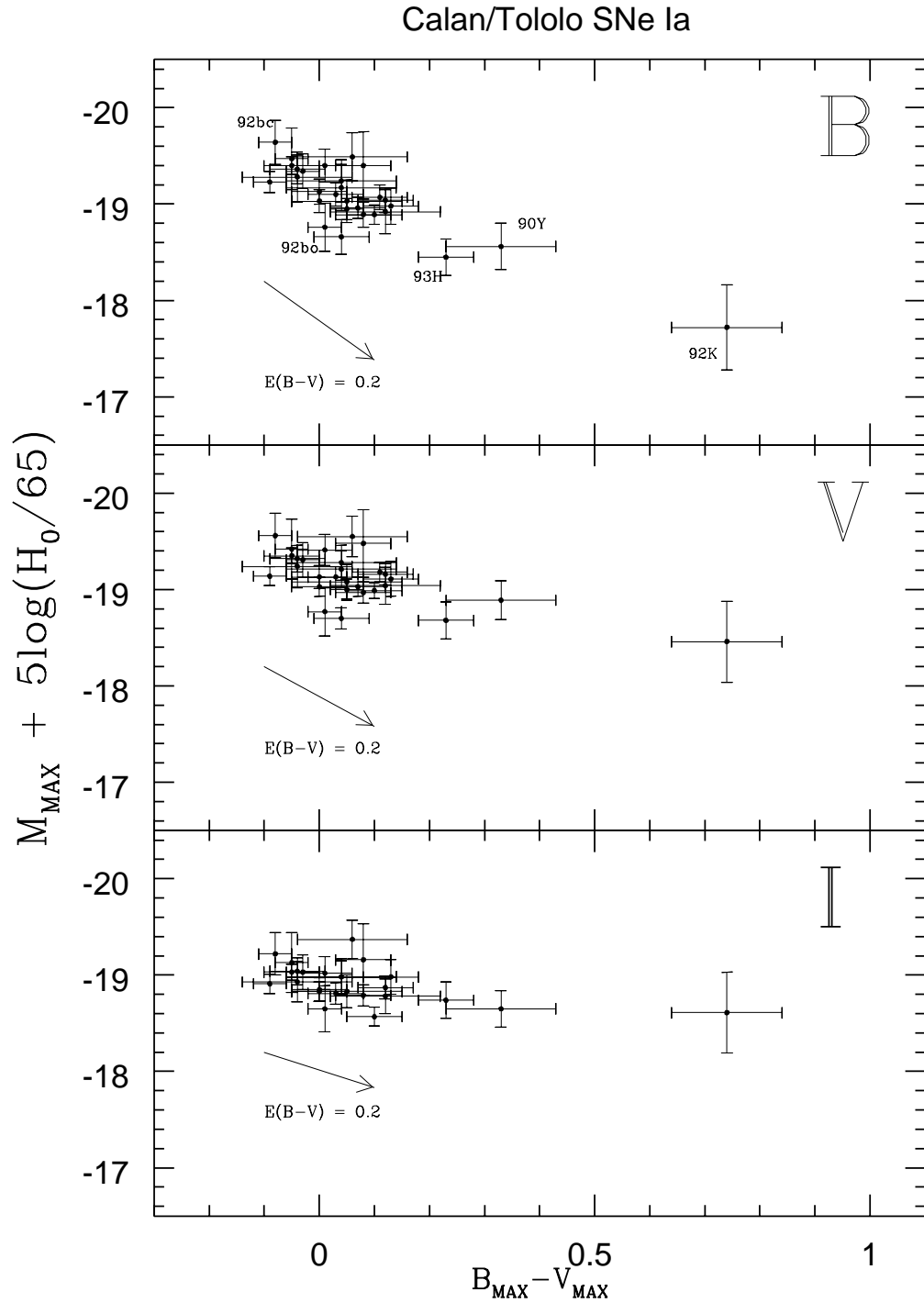


Figure 2: The absolute B, V, and I magnitudes of the Calán/Tololo sample of 29 SNe Ia, plotted as a function of their $B_{\text{MAX}} - V_{\text{MAX}}$ colors. The Galactic reddening vectors (with slopes of 4.1 in B, 3.1 in V, and 1.85 in I) corresponding to $E(B-V)=0.2$ are indicated.

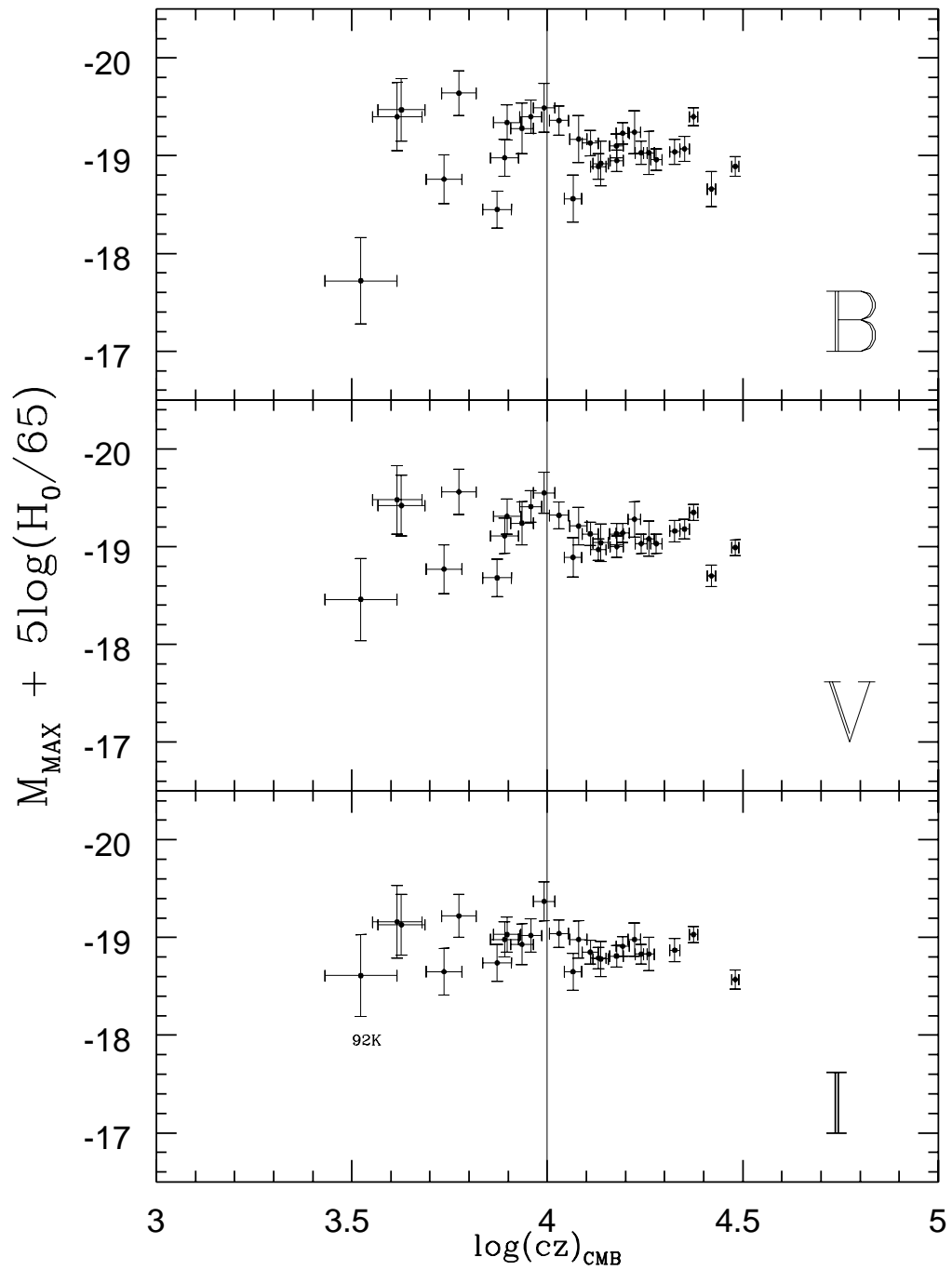


Figure 3: The absolute B, V, and I magnitudes of the Calán/Tololo SNe Ia plotted as a function of redshift. The vertical line at $\log cz = 4$ ($10,000 \text{ km s}^{-1}$) illustrates the separation of the sample into two groups.

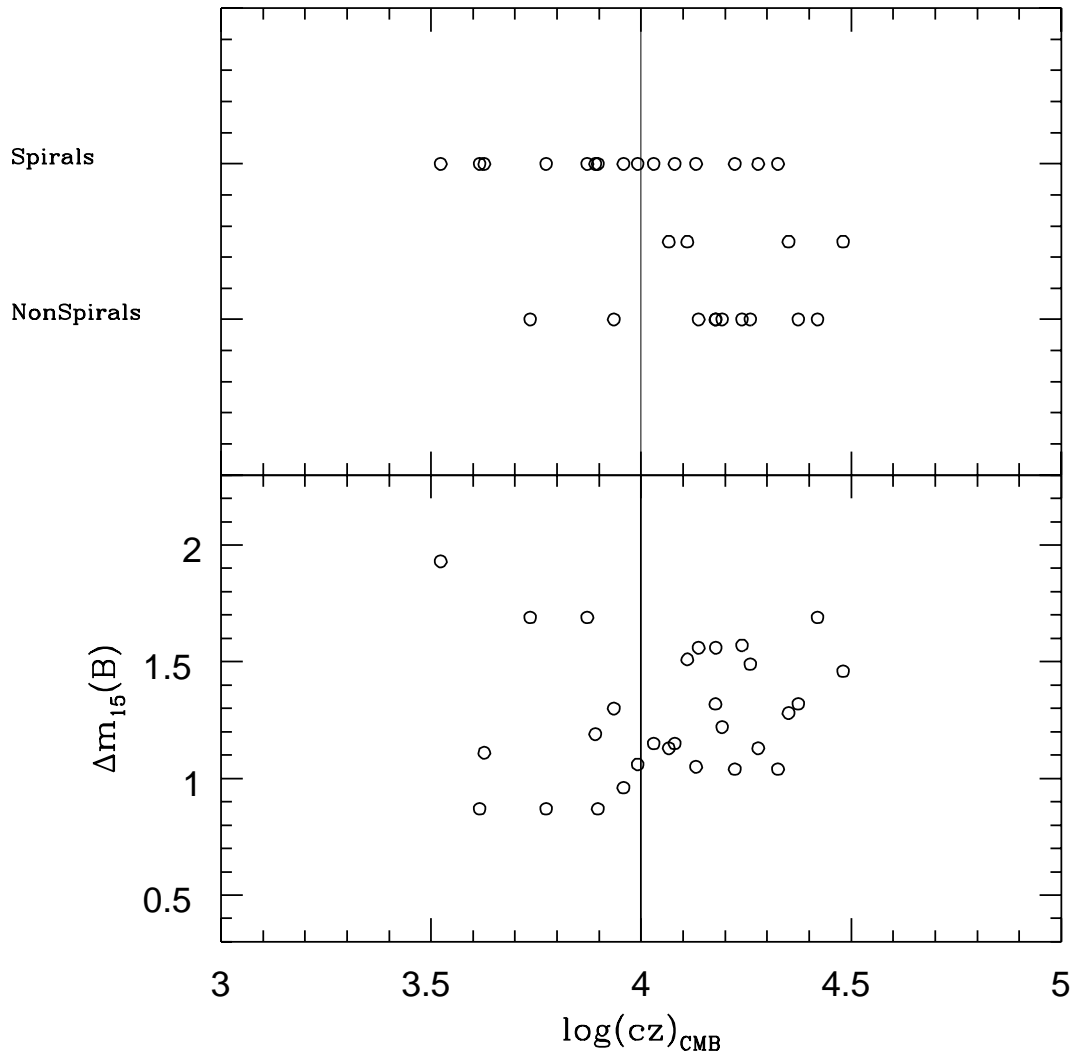


Figure 4: (top) The morphological types of their host galaxies of the Calán/Tololo SNe Ia plotted as a function of redshift. Note that the ratio of spirals/nonspirals is significantly higher in the nearby sample ($\log cz < 4$) than in the more distant group ($\log cz > 4$). (bottom) The decline rate ($\Delta m_{15}(B)$) plotted vs redshift. Note the wide spread in decline rates in the nearby sample, indicative of the full range of morphological types seen in the top panel.

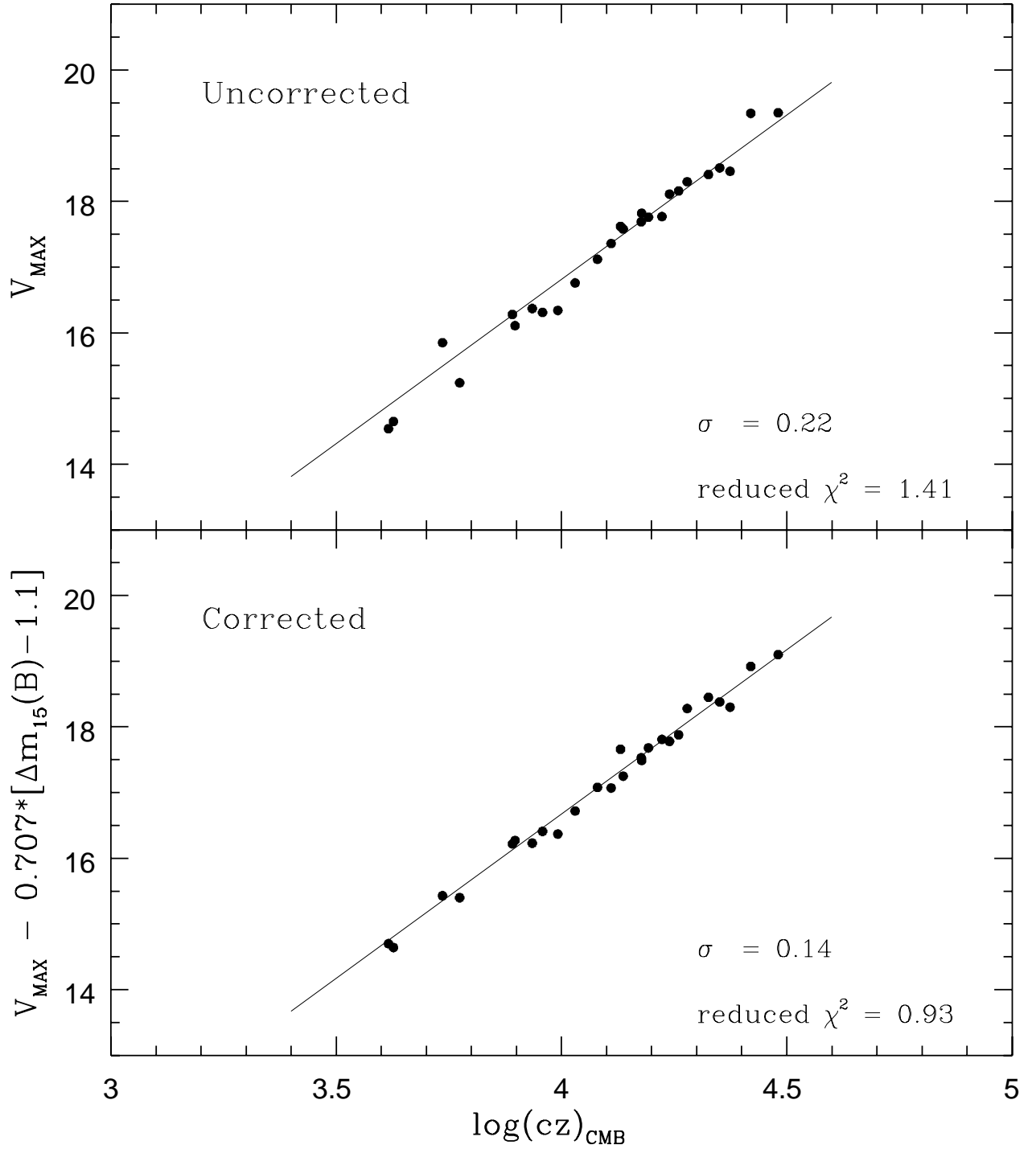


Figure 5: (top panel) The Hubble diagram in V for the SNe Ia in the Calán/Tololo sample with $B_{\text{MAX}} - V_{\text{MAX}} \leq 0.20$. (bottom panel) The Hubble diagram for the same 26 events after correction for the peak luminosity-decline rate dependence.